SIMULATION OF LAMELLIPODIAL FRAGMENTS

DIETMAR OELZ AND CHRISTIAN SCHMEISER

Abstract. A steepest descent approximation scheme is derived for a recently developed model for the dynamics of the actin cytoskeleton in the lamellipodia of living cells. The scheme is used as a numerical method for the simulation of thought experiments, where a lamellipodial fragment is pushed by a pipette, and subsequently changes its shape and position.

1. Introduction

Lamellipodia are the motility organs of many types of crawling cells. They are flat structures supported by a network of actin polymers. The modelling of their dynamic chemo-mechanical behaviour has received considerable attention recently. As examples we mention dynamic simulations based on a Potts model, where the polymer filaments locally may take one of six orientations [10], a two dimensional elastic continuum model [15], and a multiscale model [7].

The philosophy of our recent modeling approach (cp. [14], [13]) is the derivation of continuum models for the lamellipodium, based on models for individual filaments. It combines the effects of filament bending, polymerization and depolymerization, and of cytoskeleton proteins cross-linking the network and providing adhesion to the substrate. The modeling accounts for the reaction kinetics and for the mechanical effects of the latter.

The result is a multiphase evolution model for lamellipodia with arbitrary shape which allows to relate the structure and dynamics of the actin network to the traction forces and shape changes that constitute the amoeboid movement of cells. For a more detailed description of the biological phenomena and other modelling approaches we refer to [14] and [13].

After presenting the model in the remainder of this section, we formulate a numerical scheme in Section 2, namely the steepest descent approximation scheme based on solving a minimization problem in each time step. In Section 3 simulations are presented, which correspond to situations, where cells [6] or cytoplasmic fragments [17], placed on a flat substrate, assume a preferably circular form, even after deformation by external mechanical forces.

The model assumes that there is an elastic resistance against bending of actin filaments, against stretching and twisting of cross-links between the filaments, against polymerization of the barbed ends by the membrane, and against the stretching of transmembrane linkages (called adhesions) between filaments and the substrate.

The model assumes that the lamellipodium is two-dimensional and has the topology of a ring, i.e. it lies between two closed curves. Furthermore it assumes that all actin filaments belong to one of two families, called clockwise and anti-clockwise filaments. Filaments of the same family do not cross each other. Crossings of clockwise with anti-clockwise filaments are transversal. All

1991 *Mathematics Subject Classification.* Primary: 92C10 Secondary: 92C17, 92C37, 74L15, 74A25.

Key words and phrases. Modelling, Cell Movement.

This work has been supported by the Vienna Science and Technology Fund through its projects MA04-039 and MA09-004.

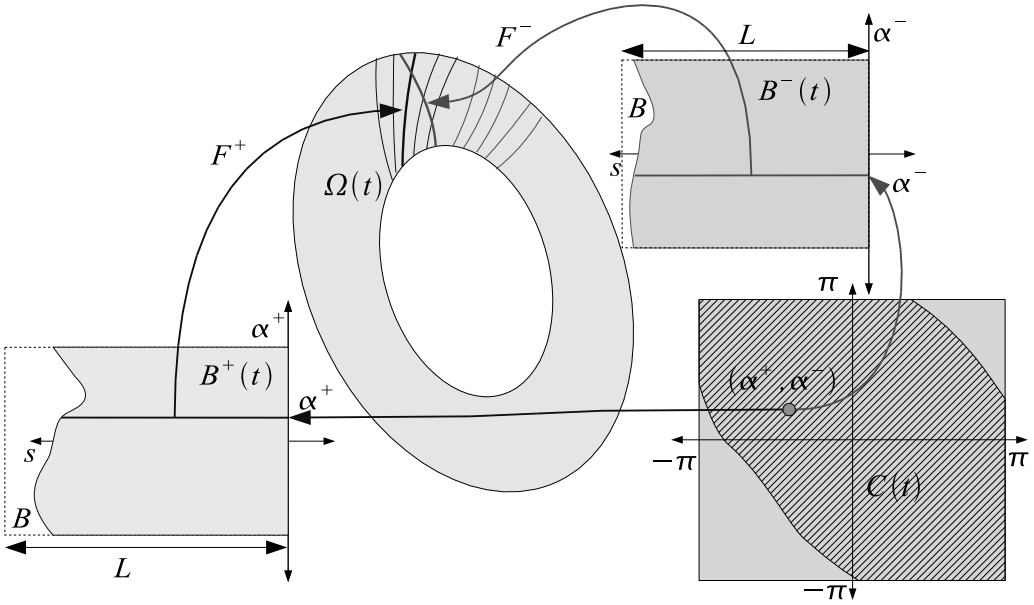

FIGURE 1. The functional framework of the model.

barbed ends touch the leading edge of the lamellipodium, i.e. the outer curve of the previous assumption. Filaments are inextensible.

As a consequence, the lamellipodium has the organization depicted in Figure 1. The model will be presented in nondimensional form (see [13] for details of the scaling). The index $\alpha \in S^1$ is used for labelling filaments, where the torus S^1 will occasionally be represented by the interval $[-\pi, \pi)$. Thus, all functions of α are assumed 2π-periodic in the following, which is a consequence of the ring topology. The position along filaments is given by the arclength parameter $s \in [-L, 0]$, where the maximal length of filaments is given by $L > 0$. Hence we define

$$B := S^1 \times [-L, 0]\,.$$

For any time $t \geq 0$, $F^+(t, \alpha, s)$ and $F^-(t, \alpha, s)$ with

$$F^\pm : [0, \infty) \times B \to \mathbb{R}^2\,,$$

describe the positions of the clockwise and, respectively, anti-clockwise filaments.

The fact that filaments of the same family do not cross, implies that $F^\pm(t, \cdot) :\ B \to \mathbb{R}^2$ has to be one-to-one. The shape of the lamellipodium at time t is given by

$$\Omega(t) = F^+(t, B) \cup F^-(t, B)\ .$$

Its boundary consists of an inner and an outer curve: $\partial\Omega(t) = \partial\Omega_{in}(t) \cup \partial\Omega_{out}(t)$. The facts that s is an arclength parameter and that all barbed ends touch the leading edge of the membrane, is translated into the two constraints

$$\begin{aligned} &|\partial_s F^+| = |\partial_s F^-| = 1\,, \\ &\partial\Omega_{out}(t) = \{F^+(t, \alpha, 0) :\ \alpha \in S^1\} = \{F^-(t, \alpha, 0) :\ \alpha \in S^1\}\,. \end{aligned} \tag{1.1}$$

Filaments polymerize at the barbed ends ($s = 0$) with given polymerization speed $v^\pm(t, \alpha)$. Since filaments are assumed inextensible, $\sigma = s + \int_0^t v^\pm(t', \alpha)dt'$ can be interpreted as a Lagrangian

variable, i.e. as a label for monomers, along the clockwise (resp. anticlockwise) filament with label α. Correspondingly, the material derivative

$$D_t^{\pm} := \partial_t - v^{\pm}\partial_s \tag{1.2}$$

is used here and in the following. Depolymerization at the pointed ends is a stochastic process with prescribed distribution. The length distributions

$$\eta^{\pm} : \ [0,\infty) \times B \to \mathbb{R}_+$$

are considered as given. They are nondecreasing functions of s, which we interpret as the number density of filaments in each index element $d\alpha$, whose length at time t is bigger than $-s$.

The model assumes that each clockwise filament crosses each anti-clockwise filament at most once. Crossings of filaments only occur in $\Omega_c(t) = F^+(t,B) \cap F^-(t,B) \subset \Omega(t)$. In terms of the filament labels, this set can also be represented by

$$\begin{aligned} \mathcal{C}(t) = \big\{ &(\alpha^+,\alpha^-) \in (S^1)^2 : \ \exists\, s^{\pm}(t,\alpha^+,\alpha^-) \text{ such that} \\ &F^+(t,\alpha^+,s^+(t,\alpha^+,\alpha^-)) = F^-(t,\alpha^-,s^-(t,\alpha^+,\alpha^-)) \big\} \, . \end{aligned} \tag{1.3}$$

Consistent with the assumption that two given filaments cross at most once, we assume that for each $(\alpha^+,\alpha^-) \in \mathcal{C}(t)$, $s^+(t,\alpha^+,\alpha^-)$ and $s^-(t,\alpha^+,\alpha^-)$ are unique. Defining the sets of potential binding sites for cross-linkers

$$B^{\pm}(t) := \{(\alpha^{\pm}, s^{\pm}(t,\alpha^+,\alpha^-)) : \ (\alpha_+,\alpha_-) \in \mathcal{C}(t)\} \subset B \, ,$$

the maps $(\alpha_+,\alpha_-) \mapsto (\alpha^{\pm}, s^{\pm}(t,\alpha^+,\alpha^-))$ from $\mathcal{C}(t)$ to $B^{\pm}(t)$ are invertible. Combining one of them with the other's inverse gives an invertible map $(\alpha^+,s^+) \mapsto (\alpha^-(t,\alpha^+,s^+), s^-(t,\alpha^+,s^+))$ from $B^+(t)$ to $B^-(t)$.

We complete the description of the geometry of crossings by defining the angle

$$\varphi(t,\alpha^+,\alpha^-) = \arccos\left[\partial_s F^+(t,\alpha^+,s^+(t,\alpha^+,\alpha^-)) \cdot \partial_s F^-(t,\alpha^-,s^-(t,\alpha^+,\alpha^-))\right] \, , \tag{1.4}$$

between crossing filaments. This will be compared to an equilibrium angle φ_0 determined by the properties of cross-linking molecules. Permitting also obtuse angles $0 \le \varphi,\, \varphi_0 \le \pi$, we allow for cross-linkers sensitive to the orientation of actin filaments.

The stochastic building and breaking of cross-links can be described as a macroscopic friction effect with friction coefficient $\mu^S[\varphi - \varphi_0]$ as well as a resistance against torsion with torsional elasticity $\mu^T[\varphi - \varphi_0]$, both possibly depending on the deviation $\varphi - \varphi_0$ from the equilibrium angle. When writing these macroscopic stiffness parameters as functions on the B-domains, it has to be taken into account that they only contribute on $B^{\pm}$, and the number of crossings per unit length $|\partial\alpha^{\mp}/\partial s^{\pm}|$ has to be considered:

$$\mu_{\pm}^S = \begin{cases} \mu^S \left|\frac{\partial\alpha^{\mp}}{\partial s^{\pm}}\right| & \text{in } B^{\pm}(t) \, , \\ 0 & \text{in } B \setminus B^{\pm}(t) \, , \end{cases} \qquad \mu_{\pm}^T = \begin{cases} \mu^T \left|\frac{\partial\alpha^{\mp}}{\partial s^{\pm}}\right| & \text{in } B^{\pm}(t) \, , \\ 0 & \text{in } B \setminus B^{\pm}(t) \, . \end{cases} \tag{1.5}$$

The building and breaking of connections to the substrate by adhesion molecules leads to a macroscopic friction effect with a constant friction coefficient μ^A. This assumes uniform distributions of possible adhesion sites across the substrate and along the filaments.

We compute the circumference $C[F^+] = C[F^-]$ of the lamellipodium, given by either one of the two equivalent formulations

$$C[F^{\pm}] := \int_{S^1} |\partial_\alpha F^{\pm}(t,\alpha,0)| \, d\alpha \, . \tag{1.6}$$

The parameter $\kappa^M > 0$ represents the resistance of the membrane against stretching beyond an equilibrium circumference C_0. The bending elasticity of actin filaments is denoted by κ^B.

The model is given by the two equations

$$\begin{aligned}(1.7)\quad &\kappa^B\partial_s^2(\eta^\pm\partial_s^2F^\pm) - \partial_s(\eta^\pm\lambda^\pm\partial_sF^\pm) + \eta^\pm\,\mu^A\,D_t^\pm F^\pm \\ &\qquad\qquad \pm\,\partial_s\left(\eta^+\eta^-\mu_\pm^T\,(\varphi-\varphi_0)\,\partial_sF^{\pm\perp}\right) \pm \eta^+\eta^-\mu_\pm^S\left(D_t^+F^+ - D_t^-F^-\right) = 0\,.\end{aligned}$$

The terms in the first row correspond to standard linear models for the deformation of beams. The first term corresponds to bending, the second to stretching (just the right amount such that $|\partial_sF^\pm| = 1$ holds), and the third to friction caused by adhesion to the substrate. All these terms are evaluated at (t,α,s) and none of them generates any coupling in α, i.e., between different filaments. The terms in the second line describe the effects of cross-linking. Note that, in the equation for F^+, the derivatives of F^- have to be evaluated at $(t,\alpha^-(t,\alpha,s),s^-(t,\alpha,s))$ and vice versa, employing the mapping between $B^+(t)$ and $B^-(t)$. The last term represents the macroscopic effect of the resistance against stretching of cross-links.

The solutions of the equations (1.7) have to satisfy the boundary conditions

$$\begin{aligned}&\kappa^B\partial_s(\eta^\pm\partial_s^2F^\pm) - \lambda^\pm\partial_sF^\pm \pm \mu_\pm^T(\varphi-\varphi_0)\partial_sF^{\pm\perp} \\ &\qquad\qquad = \pm\lambda^\pm_{\rm edge}\nu - \kappa^M\,(C^\pm - C_0)_+\,\partial_\alpha\left(\tfrac{\partial_\alpha F^\pm}{|\partial_\alpha F^\pm|}\right), \quad \text{for } s=0\,, \\ &-\kappa^B\partial_s(\eta^\pm\partial_s^2F^\pm) + \eta^\pm\lambda^\pm\partial_sF^\pm \mp \eta^+\eta^-\mu_\pm^T(\varphi-\varphi_0)\partial_sF^{\pm\perp} = 0\,, \quad \text{for } s=-L\,, \\ &\eta^\pm\partial_s^2F^\pm = 0\,, \quad \text{for } s=-L,\,0\,.\end{aligned} \tag{1.8}$$

The Lagrange parameters $\lambda^\pm(t,\alpha,s)$ and $\lambda^-_{\rm edge}(t,\alpha) = \lambda^+_{\rm edge}(t,\alpha^+(t,\alpha,0))$ have to be determined such that the constraints (1.1) are satisfied.

The weak formulation of (1.7), (1.8) is given by

$$\begin{aligned}&\int_{S^1}\left[\kappa^M\left(C^\pm-C_0\right)_+\frac{\partial_\alpha F^\pm}{|\partial_\alpha F^\pm|}\cdot\partial_\alpha\delta F^\pm \pm \lambda^\pm_{\rm edge}\nu\cdot\delta F^\pm\right]_{s=0} d\alpha \\ &\pm\int_{\mathcal{C}(t)}\left(\mu^S(D_tF^+ - D_tF^-)\cdot\delta F^\pm - \mu^T(\varphi-\varphi_0)\partial_sF^{\pm\perp}\cdot\partial_s\delta F^\pm\right)\eta^+\eta^-\,d(\alpha^+,\alpha^-) \\ &+\int_B\left(\kappa^B\partial_s^2F^\pm\cdot\partial_s^2\delta F^\pm + \mu^AD_t^\pm F^\pm\cdot\delta F^\pm + \lambda^\pm\partial_sF^\pm\cdot\partial_s\delta F^\pm\right)\eta^\pm\,d(\alpha,s) = 0\,,\end{aligned} \tag{1.9}$$

with the test functions $\delta F^\pm : B \mapsto \mathbb{R}^2$. The first integral corresponds to the leading edge and contributes to the first boundary condition in (1.8). The remaining boundary conditions are the natural conditions modelling the absence of a linear force acting on the pointed ends and of a moment of momentum at either end. From the second and the third integral, the system (1.7) is derived. For that purpose the integration domain $\mathcal{C}(t)$ has to mapped to B. Noting that in the second integral $F^\pm$ and $\delta F^\pm$ and their derivatives are evaluated at $(t,\alpha^\pm,s^\pm)$, we employ the transformations $(\alpha^+,\alpha^-)\mapsto(\alpha,s) = (\alpha^\pm, s^\pm(t,\alpha^+,\alpha^-))$, which yields the additional coefficients in (1.5).

2. Numerical scheme

In this section we will present an approximation scheme for solutions of the system (1.7), (1.8), (1.1). It is derived from the usual steepest descent approximation scheme for gradient flows. (cp. [3, 2] and [1]). Let

$$A := \left\{G:\ B\to\mathbb{R}^2 : |\partial_sG| \equiv 1\right\}\,, \tag{2.1}$$

then we define the set of admissible network configurations $\mathcal{A}$ as

$$\mathcal{A} := \left\{(G^+, G^-) \in A \times A : \ \{G^+(\alpha, 0) : \ \alpha \in S^1\} = \{G^-(\alpha, 0) : \ \alpha \in S^1\}\right\} , \tag{2.2}$$

which represents the set of all network configurations that satisfy the constraints (1.1).

Let $\tau > 0$ be the constant size of the time steps and $t_n = n\tau$, $n = 0, 1, ...$, the discrete times. By $F_n^{\pm}(\alpha, s)$ we denote discrete approximations for $F^{\pm}(t_n, \alpha, s)$. We also use the abbreviations $\eta_n^{\pm}(\alpha, s) = \eta^{\pm}(t_n, \alpha, s)$ and $v_n^{\pm}(\alpha) = v^{\pm}(t_n, \alpha)$. As an approximation of $\mathcal{C}(t_{n-1})$ we define $\mathcal{C}_{n-1}$ as the set of pairs (α^+, α^-), such that $s_{n-1}^{\pm}(\alpha^+, \alpha^-) \in [-L, 0]$ exist, satisfying

$$F_{n-1}^+(\alpha^+, s_{n-1}^+) = F_{n-1}^-(\alpha^-, s_{n-1}^-) . \tag{2.3}$$

The angle $\varphi_{n-1}(\alpha^+, \alpha^-)$ is defined by (1.4) in terms of $\partial_s F_{n-1}^{\pm}(\alpha^{\pm}, s_{n-1}^{\pm})$. We also define $\mu_{n-1}^S = \mu^S[\varphi_{n-1} - \varphi_0]$ and $\mu_{n-1}^T = \mu^T[\varphi_{n-1} - \varphi_0]$.

Starting with initial data $(F_I^+, F_I^-) \in \mathcal{A}$, we define the sequence (F_n^+, F_n^-) by the recursive scheme

$$(F_0^+, F_0^-) = (F_I^+, F_I^-) \quad \text{and} \quad (F_n^+, F_n^-) = \operatorname{argmin}_{(G^+,G^-)\in\mathcal{A}} U^n[G^+, G^-] . \tag{2.4}$$

Mathematically, the scheme (2.4) assumes that the filament positions minimize a potential energy functional containing contributions from elastic and dissipative effects,

$$\begin{aligned} U^n[G^+, G^-] :=& U_{\text{bending}}^{+,n}[G^+] + U_{\text{bending}}^{-,n}[G^-] + U_{\text{scl}}^n[G^+, G^-] + U_{\text{tcl}}^n[G^+, G^-] \\ &+ U_{\text{membrane}}[G^+, G^-] + U_{\text{adh}}^{+,n}[G^+] + U_{\text{adh}}^{-,n}[G^-] , \end{aligned} \tag{2.5}$$

where

$$\begin{aligned} U_{\text{membrane}}[G^+, G^-] &:= \kappa^M \left(\frac{C[G^+] + C[G^-]}{2} - C_0 \right)_+^2 , \\ U_{\text{bending}}^{\pm,n}[G] &:= \frac{\kappa^B}{2} \int_B |\partial_s^2 G|^2 \eta_n^{\pm} \, d(\alpha, s) , \\ U_{\text{scl}}^n[G^+, G^-] &:= \frac{1}{2\tau} \int_{\mathcal{C}_{n-1}} \mu_{n-1}^S \left| G^+\left(\alpha^+, s_{n-1}^+ - v_n^+\tau\right) - G^-\left(t, \alpha^-, s_{n-1}^- - v_n^-\tau\right) \right|^2 \\ &\qquad \eta_n^+ \eta_n^- \, d(\alpha^+, \alpha^-) , \\ U_{\text{tcl}}^n[G^+, G^-] &:= \frac{1}{2} \int_{\mathcal{C}_{n-1}} \mu_{n-1}^T \left(\arccos\left(\frac{\partial_s G^+}{|\partial_s G^+|}(\alpha^+, s_{n-1}^+) \cdot \frac{\partial_s G^-}{|\partial_s G^-|}(\alpha^-, s_{n-1}^-) \right) \right. \\ &\qquad \left. - \varphi_0 \right)^2 \eta_n^+ \eta_n^- \, d(\alpha^+, \alpha^-) , \\ U_{\text{adh}}^{\pm,n}[G] &:= \frac{1}{2\tau} \int_B \mu^A \left| G\left(\alpha, s - v_n^{\pm}\tau\right) - F_{n-1}^{\pm}\left(\alpha, s\right) \right|^2 \eta_n^{\pm} \, d(\alpha, s) . \end{aligned} \tag{2.6}$$

Lemma 1. *The one-step scheme defined by* (2.4)–(2.6) *is a consistent method for solving* (1.9) *subject to the initial conditions* $F^{\pm}(t = 0) = F_I^{\pm}$.

Proof. The displacements $F_n^{\pm}$ have to satisfy the variational equations

$$\delta U^n[F_n^+, F_n^-](\delta F^+, \delta F^-) = 0 \tag{2.7}$$

for all admissible variations $(\delta F^+, \delta F^-)$, where δU^n is the variation of the total energy (2.5). Admissibility conditions for the variations are a consequence of the constraints (1.1). Since this

leads to rather inconvenient equations, a Lagrange multiplier approach is used instead, with the additional Lagrangian functionals

$$U^{\pm,n}_{\rm ext}[G^\pm] = \frac{1}{2}\int_B \lambda^\pm \left(|\partial_s G^\pm|^2 - 1\right) \eta^\pm_n \, d(\alpha,s)\,,$$

and

$$U_{\rm edge}[G^+,G^-] = \int_{S^1} \lambda_{\rm edge}(\alpha^+)(G^+(\alpha^+,0) - G^-(\hat\alpha(\alpha^+),0))\cdot\nu(\alpha^+)\,d\alpha^+\,,$$

where $\nu(\alpha^+)$ is the unit outward normal vector along the barbed ends of the clockwise filaments (i.e. orthogonal to $\partial_\alpha G^+(\alpha^+,0)$) and $\hat\alpha(\alpha^+)$ is such that $(G^+(\alpha^+,0) - G^-(\hat\alpha(\alpha^+),0))$ is parallel to $\nu(\alpha^+)$ (cp. [13] for more details).

The variational equation now becomes

$$\left(\delta U^n[F^+_n,F^-_n] + \delta U^{+,n}_{\rm ext}[F^+_n] + \delta U^{-,n}_{\rm ext}[F^-_n] + \delta U_{\rm edge}[F^+_n,F^-_n]\right)(\delta F^+,\delta F^-) = 0\,, \tag{2.8}$$

where δF^+ and δF^- are unrestricted test functions. We claim that (2.8) is consistent with (1.9) in the limit $\tau\to 0$. This will be shown by computing the variation and by carrying out the limit for each energy contribution individually after substituting $F_n(\alpha,s) = F(t,\alpha,s)$, $F_{n-1}(\alpha,s) = F(t-\tau,\alpha,s)$ with a smooth function F.

(1) For the resistance against stretching the membrane, we obtain

$$\lim_{\tau\to 0}\delta U_{\rm membrane}[F^\pm_n]\delta F^\pm = \kappa^M\left(C[F^\pm]-C_0\right)_+ \int_{S^1}\frac{\partial_\alpha F^\pm(s=0)}{|\partial_\alpha F^\pm(s=0)|}\cdot\partial_\alpha\delta F^\pm(s=0)\,d\alpha\,. \tag{2.9}$$

(2) The bending energy of the filaments gives

$$\lim_{\tau\to 0}\delta U^{\pm,n}_{\rm bending}[F^\pm_n]\delta F^\pm = \kappa^B\int_B\left(\partial_s^2 F^\pm\cdot\partial_s^2\delta F^\pm\right)\eta^\pm\,d(\alpha,s)\,. \tag{2.10}$$

(3) The variation of the energy contribution by stretching the cross-links is given by

$$\begin{aligned}\delta U^n_{\rm scl}[F^+_n,F^-_n]\delta F^\pm &= \pm\frac{1}{\tau}\int_{\mathcal{C}_{n-1}}\left(F^+_n\left(\alpha^+,s^+_{n-1}-v^+_n\tau\right)-F^-_n\left(\alpha^-,s^-_{n-1}-v^-_n\tau\right)\right)\\ &\qquad\cdot\delta F^\pm(\alpha^\pm,s^\pm_{n-1}-v^\pm_n\tau)\,\eta^+_n\eta^-_n\mu^S_{n-1}\,d(\alpha^+,\alpha^-)\,.\end{aligned}$$

Using (2.3), the term in parentheses can be written as

$$\begin{aligned}&F^+_n(\alpha^+,s^+_{n-1}-v^+_n\tau)-F^+_{n-1}(\alpha^+,s^+_{n-1}-v^+_n\tau)+F^+_{n-1}(\alpha^+,s^+_{n-1}-v^+_n\tau)-F^+_{n-1}(\alpha^+,s^+_{n-1})\\ &+F^-_{n-1}(\alpha^-,s^-_{n-1})-F^-_{n-1}(\alpha^-,s^-_{n-1}-v^-_n\tau)+F^-_{n-1}(\alpha^-,s^-_{n-1}-v^-_n\tau)-F^-_n(\alpha^-,s^-_{n-1}-v^-_n\tau)\,.\end{aligned}$$

Therefore passing to the limit $\tau\to 0$ gives

$$\lim_{\tau\to 0}\delta U_{\rm scl}[F^+_n,F^-_n]\delta F^\pm = \pm\int_{\mathcal{C}(t)}\mu^S(D^+_tF^+ - D^-_tF^-)\cdot\delta F^\pm\,\eta^+\eta^-\,d(\alpha^+,\alpha^-)\,. \tag{2.11}$$

(4) For the computation of the variation of the twisting energy we use the identity $\left(\delta\frac{x}{|x|}\right)_{|x|=1} = (x^\perp\cdot\delta x)x^\perp$ (with the orthogonal vector $(x_1,x_2)^\perp = (-x_2,x_1)$). We obtain

$$\begin{aligned}\delta\arccos\left(\frac{\partial_sF^+_n}{|\partial_sF^+_n|}\cdot\frac{\partial_sF^-_n}{|\partial_sF^-_n|}\right)\delta F^\pm &= -\frac{(\partial_sF^{\pm\perp}_n\cdot\partial_sF^\mp_n)(\partial_sF^{\pm\perp}_n\cdot\partial_s\delta F^\pm)}{\sin\varphi_n}\\ &= \mp\partial_sF^{\pm\perp}_n\cdot\partial_s\delta F^\pm\,,\end{aligned}$$

where $\partial_s F_n^\pm$ and $\partial_s \delta F^\pm$ are evaluated at $(\alpha^\pm, s_{n-1}^\pm)$. This implies

$$\lim_{\tau\to 0} \delta U_{\mathrm{tcl}}^n[F_n^+, F_n^-]\delta F^\pm = \mp \int_{\mathcal{C}(t)} \mu^T(\varphi-\varphi_0)(\partial_s F^{\pm\perp}\cdot\partial_s\delta F^\pm)\eta^+\eta^- \, d(\alpha^+,\alpha^-)\,, \tag{2.12}$$

where now $\partial_s F^\pm$ and $\partial_s \delta F^\pm$ are evaluated at $(t, \alpha^\pm, s^\pm)$.

(5) The variation of the stretching energy of the adhesions is straightforward and reads

$$\begin{aligned}\delta U_{\mathrm{adh}}^{\pm,n}[F_n^\pm]\delta F^\pm &= \frac{1}{\tau}\int_B \mu^A \left(F_n^\pm(\alpha, s - v_{n-1}^\pm\tau) - F_{n-1}^\pm(\alpha,s)\right)\\ &\qquad \cdot \delta F^\pm\left(\alpha, s - v_{n-1}^\pm\tau\right)\, \eta_n^\pm \, d(\alpha,s)\,.\end{aligned}$$

In the limit $\tau \to 0$, a material derivative occurs similarly to the stretching of the cross-links:

$$\lim_{\tau\to 0} \delta U_{\mathrm{adh}}^\pm[F_n^\pm]\delta F^\pm = \int_B \mu^A D_t^\pm F^\pm \cdot \delta F^\pm \, \eta^\pm \, d(\alpha,s)\,. \tag{2.13}$$

Adding the contributions (2.9)–(2.13) completes the proof. □

3. Simulations

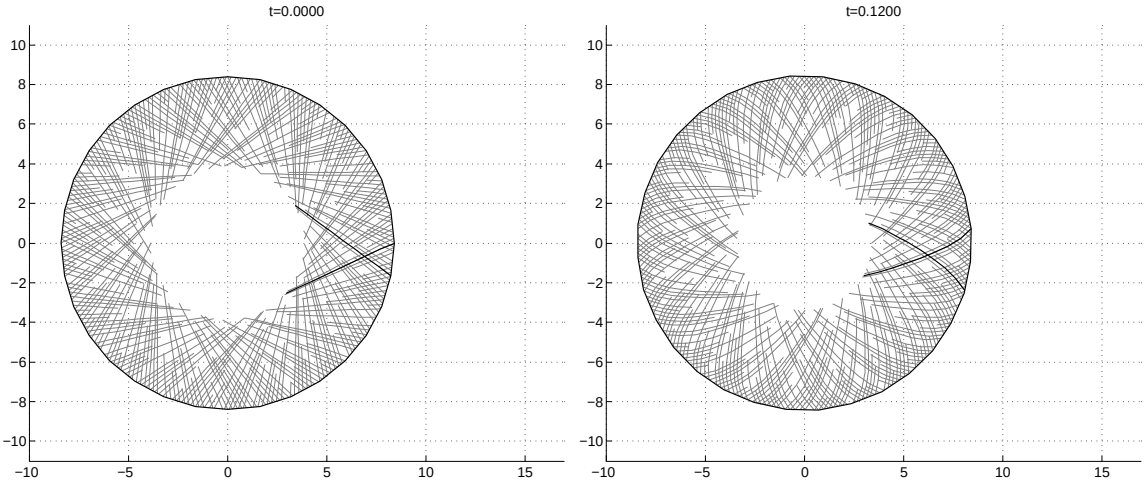

Figure 2. Initial data and solution at time $t = 0.12\,\mathrm{min}$ with the number values of of the spatial grid in μm.

For the purpose of numerical computations, we add an additional component to the energy functional. It is meant to be a rough model for outer forces acting on the lamellipodium.

In the first case we assume that the additional component of the energy functional is given by

$$U_{\mathrm{push},1}[G^\pm] := \frac{\kappa^{P,1}}{2}\int_{S^1} (G_x^\pm)_-^2 (\partial_\alpha G_y^\pm)_\pm \, d\alpha\,, \tag{3.1}$$

where we refer to the membrane represented by either $\alpha \mapsto G^+(\alpha,0)$, which describes the membrane in the clockwise sense, or $\alpha \mapsto G^-(\alpha,0)$ describing the membrane in the anti-clockwise sense. The subscripts $(.)_\pm$ represent the modulus of the positive and negative part respectively and the subscripts $._x$ and $._y$ denote the first and second component respectively of the vector.

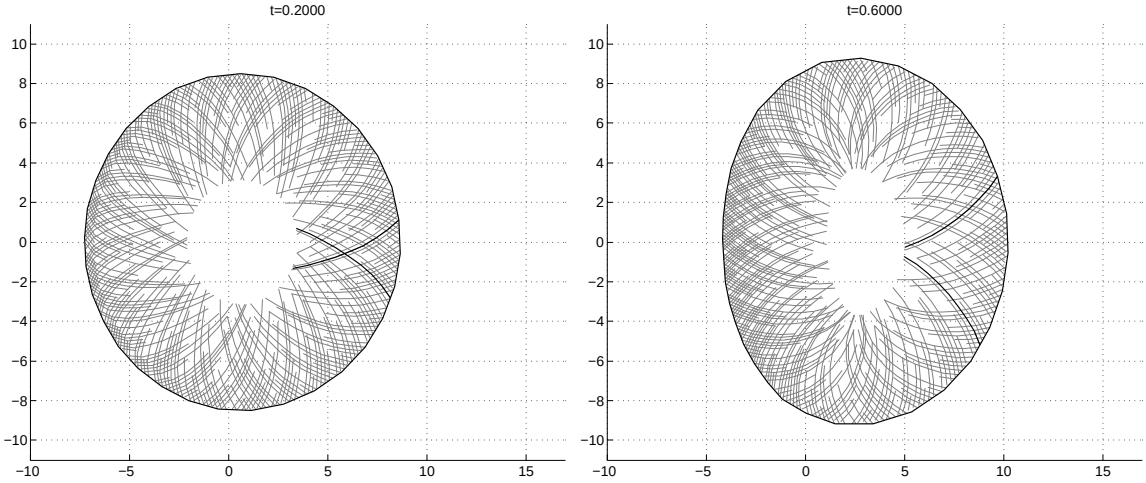

FIGURE 3. Linearly decreasing pushing force: solutions at times $t = 0.2\,\mathrm{min}$ and $t = 0.6\,\mathrm{min}$.

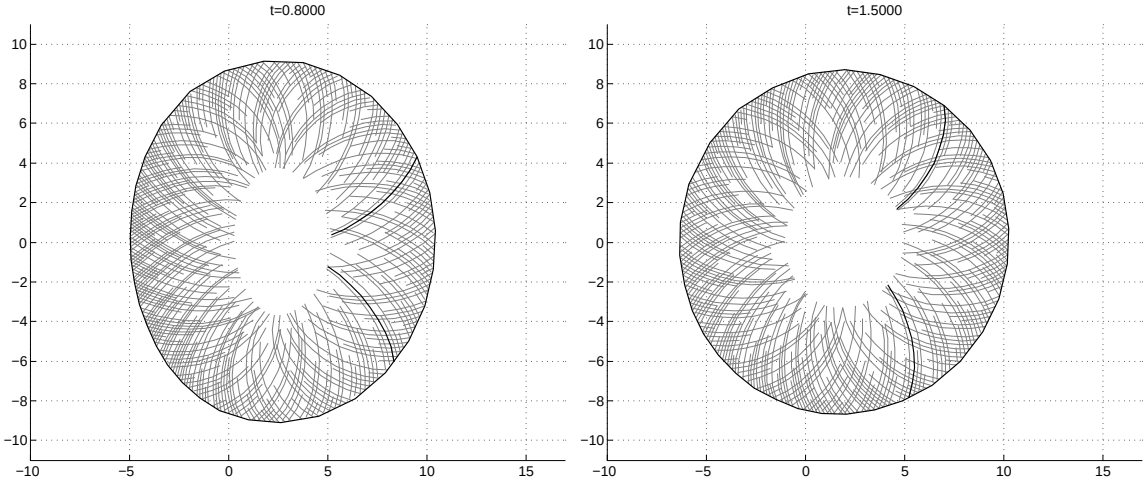

FIGURE 4. Linearly decreasing pushing force: solutions at times $t = 0.8\,\mathrm{min}$ and $t = 1.5\,\mathrm{min}$ (almost quasi-equilibrium situation).

The functional (3.1) models pushing forces from the left which decrease linearly to become zero at $x = 0$ and which act on those components of the membrane that are directed towards the left hand side.

In a second numerical experiment we assume that the additional component to the energy functional is given by

$$U_{\mathrm{push},2}[G^{\pm}] := \frac{\kappa^{P,2}}{2} \int_{S^1} (-G_x^{\pm})(\partial_\alpha G_y^{\pm})_{\pm}\, d\alpha \;, \tag{3.2}$$

which is meant to model constant pushing forces from the left again acting on those components of the membrane that are directed towards the left hand side.

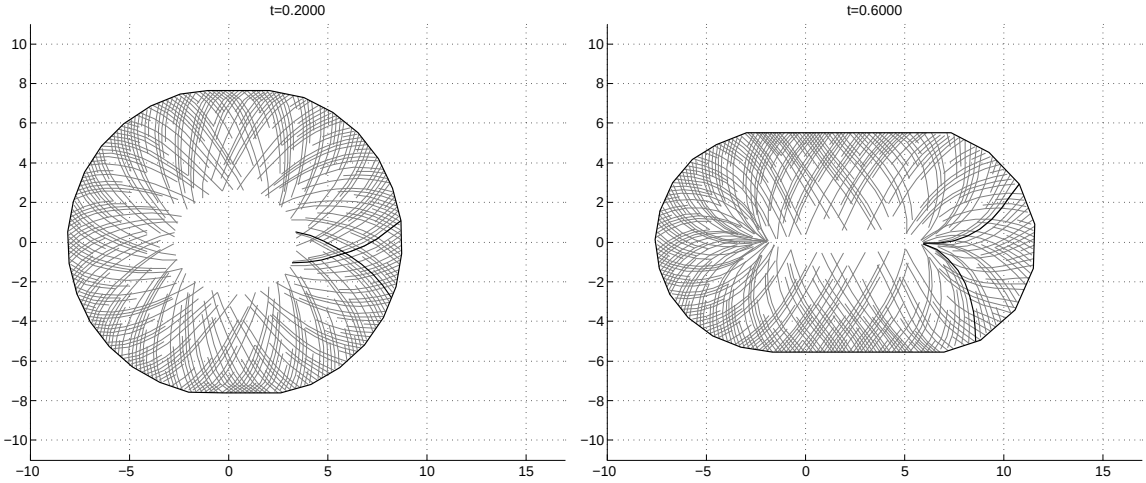

FIGURE 5. Constant pushing force: solutions at times $t = 0.2\,\text{min}$ and $t = 0.6\,\text{min}$.

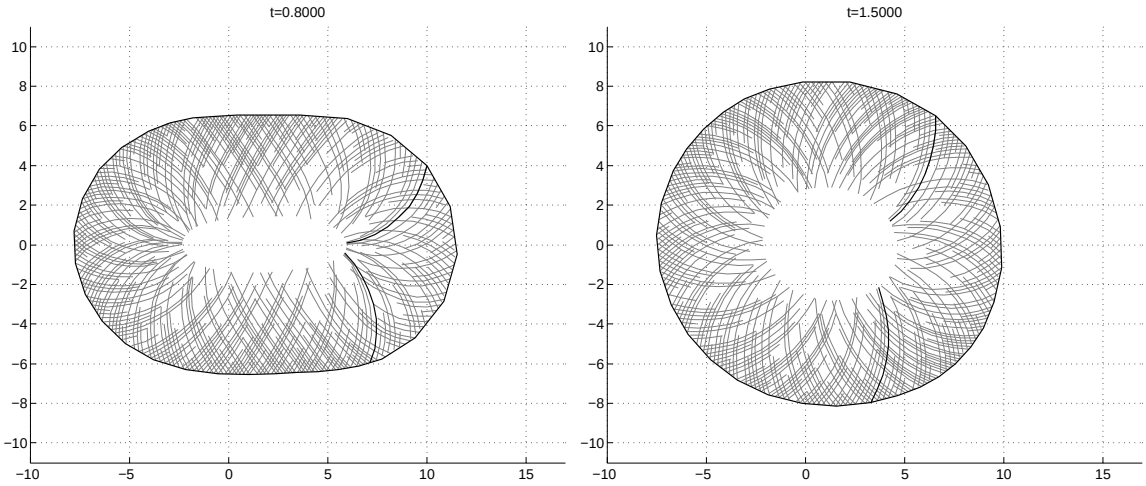

FIGURE 6. Constant pushing force: solutions at times $t = 0.8\,\text{min}$ and $t = 1.5\,\text{min}$.

The fact that we can model additional phenomena by adding additional energy components illustrates the flexibility of the present modelling approach. In order to do numerical experiments, it is even not necessary to go through the analysis part above. We rather implement the time step approximation (2.4) minimising at every time-step the sum of (2.5) and either (3.1) or (3.2).

The constraints (1.1) are enforced by choosing an appropriate parametrization of the functions G_- and G_+,

$$G^-(\alpha, s) = b^-(\alpha) - \int_s^0 \begin{pmatrix} \cos(\phi^-(\alpha, \tilde{s})) \\ \sin(\phi^-(\alpha, \tilde{s})) \end{pmatrix} d\tilde{s}$$

Description	Symbol	Value	Reference
Total number of filaments	$\#F$	4400	[8]
Number density of filaments with length $\geq -s$.	$\eta^{\pm}(t,\alpha,s)$	$\frac{1}{2\pi}\frac{\#F}{2}(1.0+3/20s)$	
Equilibrium circumference of the membrane	C_0	$8\times 2\pi\,\mu m$	
Maximal length of filaments	L	$6\,\mu m$	
Polymerization rate	$v^{\pm}(t,\alpha)$	$8\,\mu m\,\mathrm{min}^{-1}$	
Equilibrium angle of cross-links	φ_0	70°	
Elasticity of the membrane	κ^M	$911.25\,pN\,\mu m^{-1}$	[14]
Bending elasticity of one filament	κ^B	$0.07\,pN\,\mu m^2$	[4]
Macroscopic friction mediated by integrin bonds	μ^A	$0.1367\,pN\,\mathrm{min}\,\mu m^{-2}$	[11, 9]; estimation in [14]; computation of macroscopic parameters in [13, 12].
Macroscopic friction mediated by cross-linker proteins at one filament crossing	μ^S	$19.006\,pN\,\mathrm{min}\,\mu m^{-1}$	[16, 5], computation in [13, 12].
Macroscopic effect of torsional stiffness of cross-linker proteins at one filament crossing	μ^T	$0.21495\,pN\,\mu m$	[14, 5]; together with computation in [13, 12]
Force parameter in Scenario 1	$\kappa^{E,1}$	$154.0\,pN\,\mu m^{-2}$	
Force parameter in Scenario 2	$\kappa^{E,2}$	$924.0\,pN\,\mu m^{-1}$	

TABLE 1. List of parameters and literature sources.

for a vector valued function $b^- = b^-(\alpha) \in \mathbb{R}^2$ and a scalar valued function $\phi^- : B \mapsto \mathbb{R}$ and

$$G^+(\alpha,s) = b^-(\omega(\alpha)) - \int_s^0 \begin{pmatrix}\cos(\phi^+(\alpha,\tilde{s}))\\ \sin(\phi^+(\alpha,\tilde{s}))\end{pmatrix} d\tilde{s}$$

for scalar valued functions $\omega(\alpha)$ and $\phi^+ : B \mapsto \mathbb{R}$.

All the parameters with their respective interpretations are listed in Table 1. Many of them have already been used in [14] to simulate the original microscopic model in the special case of rotational symmetry.

We make the simplifying assumption that the polymerization rates $v^{\pm}$ and the length distributions $\eta^{\pm}$ are time-independent and do neither vary with respect to the filament index $\alpha \in S^1$, nor between clockwise and anti-clockwise filaments, i.e. $v^p m(t,\alpha) = v = \text{const}$ and $\eta^{\pm}(t,\alpha,s) = \eta(s)$. This allows for a rotationally symmetric steady state (without pushing forces). Furthermore the length distribution $\eta(s)$ is assumed to be uniformly positive with a strictly positive value at $s = -L$, i.e. we assume a fraction of filaments to be longer than L but neglect the mechanical effect of the excess parts.

We compute the macroscopic parameters which describe the effect of the cross-links, $\mu^S[\varphi-\varphi_0]$ and $\mu^T[\varphi-\varphi_0]$, using the formulas given in [13, 12] omitting their possible dependence on the deviation from the equilibrium angle. Finally we use the same argumentation as in [12] to determine the value of μ^A, the macroscopic friction mediated by integrin bonds.

For the numerical computations we use a uniform grid with $N = 9$ points in s-direction and $M = 32$ points in α-direction. The contributions of cross-links in (2.6), namely $U^n_{\mathrm{scl}}[G^+, G^-]$ and $U^n_{\mathrm{tcl}}[G^+, G^-]$, are not evaluated as integrals on $\mathcal{C}_{n-1}$. Instead, using the transformed densities of cross-links (1.5), they are evaluated on $B^+_{n-1} := B^+(t_{n-1})$ and on $B^-_{n-1} := B^-(t_{n-1})$ and finally the average of the two values is taken. This special treatment guarantees that the network stabilizing effect of cross-linkers, which we already observed in [14], is not inhibited by the discretization.

We visualize the lamellipodium by a random sample of the filament length distribution η combined with the information on the geometry $F^{\pm}_n$. This way we can create a realistic impression of filament shape and density at every point within the lamellipodium, whereas the numerical computations are done on the basis of 2×32 discrete filaments of length L.

We start with the pushing force initially being switched off. The initial condition and the lamellipodium after a short period of relaxation is shown in figure 2. In this figure, like in all the following figures, the scaling of the spatial grid is given in μm.

The linearly decreasing pushing force due to the quadratic potential (3.1) is then switched on at $t = 0.15\,\mathrm{min}$ and initiates a slow movement combined with a gradual deformation which can be observed at time $t = 0.2\,\mathrm{min}$ and, more intensively, at $t = 0.6\,\mathrm{min}$ (Figure 3). We observe a horizontal compression of the lamellipodium since the potential (3.1) penalizes far left positions of the membrane. Finally, at $t = 0.6\,\mathrm{min}$ the pushing force is again switched off and we observe that the shape of the lamellipodium gradually relaxes towards a circular shape as shown at $t = 1.5\,\mathrm{min}$ (Figure 4).

We remark that the observed deformation is not of elastic nature, although the shape becomes round again after the applied force ceases to be active. The round shape is actually not stabilized by the network-dynamics but by the membrane model which mimics an elastic rubber band and which therefore generates forces that prefer the circular shape.

We also perform a second numerical simulation in which we change the characteristics of the pushing force, this time using the linear potential (3.2) mimicking constant force, which we switch on and off at the same times as before. The initial evolution therefore coincides with the one of the previous setting (Figure 2). The constant pushing force again triggers a slow movement to the right, but a deformation which mostly consists in vertical compression (Figure 5). This can be easily explained by the fact that the linear potential (3.2) is most effectively avoided by reducing the surface components which are directed towards the left hand side and of course by displacement to the right against integrin-mediated friction. The relaxation to a roundish shape (Figure 6) after switching off the pushing at $t = 0.6\,\mathrm{min}$ is analogous to the previous situation.

Apart from the change in shape and the movement, the filaments perform "lateral flow", i.e. those pointing in clockwise direction move in clockwise direction and those pointing in anti-clockwise direction move in anti-clockwise direction. Two specific filaments are highlighted in all the frames to illustrate this behaviour.

In fact, in both cases we do not expect a return to a perfect circle because pushing seems to slightly modify the density of filaments due to a change in geometry and therefore lateral flow speed. This effect seems to be stronger in the case of constant force and can be observed in Figure 6 in terms of a local difference in density between clockwise and anticlockwise filaments. We suppose that this implies a slightly inhomogeneous force distribution around the membrane and thus inhibits the return to a perfect circular shape.

References

1. Luigi Ambrosio, Nicola Gigli, and Giuseppe Savaré, *Gradient flows in metric spaces and in the space of probability measures*, Lectures in Mathematics ETH Zürich, Birkhäuser Verlag, Basel, 2005.
2. Ennio De Giorgi, *New problems on minimizing movements*, Boundary value problems for partial differential equations and applications, RMA Res. Notes Appl. Math., vol. 29, Masson, Paris, 1993, pp. 81–98.
3. Ennio De Giorgi, Antonio Marino, and Mario Tosques, *Problems of evolution in metric spaces and maximal decreasing curve*, Atti Accad. Naz. Lincei Rend. Cl. Sci. Fis. Mat. Natur. (8) **68** (1980), no. 3, 180–187.
4. F. Gittes, B. Mickey, J. Nettleton, and J. Howard, *Flexural rigidity of microtubules and actin filaments measured from thermal fluctuations in shape*, J. of Cell Biology **120** (1993), 923–934.
5. W.H. Goldmann and G. Isenberg, *Analysis of filamin and [alpha]-actinin binding to actin by the stopped flow method*, FEBS Letters **336** (1993), no. 3, 408 – 410.
6. John H. Henson, Tatyana M. Svitkina, Andrew R. Burns, Heather E. Hughes, Kenneth J. MacPartland, Ronniel Nazarian, and Gary G. Borisy, *Two components of actin-based retrograde flow in sea urchin coelomocytes*, Molecular Biology of the Cell **10** (1999), 4075–4090.
7. Y. J. Kim, H Othmer, and M. Stolarska, *Multi-scale models of cell and tissue dynamics*, Phil. Trans. Roy. Soc. A **367** (2009), no. 1902, 3525–3553.
8. S.A. Koestler, S. Auinger, M. Vinzenz, K. Rottner, and J.V. Small, *Differentially oriented populations of actin filaments generated in lamellipodia collaborate in pushing and pausing at the cell front.*, Nat Cell Biol. **10** (2008), 306–313.
9. Feiya Li, Sambra D. Redick, Harold P. Erickson, and Vincent T. Moy, *Force measurements of the $\alpha_5\beta_1$ integrin-fibronectin interaction*, Biophysical Journal **84** (2003), no. 2, 1252 – 1262.
10. A. F. M. Marée, A. Jilkine, A. Dawes, V. A. Grieneisen, and L. Edelstein-Keshet, *Polarization and movement of keratocytes: a multiscale modelling approach.*, Bull. Math. Biol. **68** (2006), no. 5, 1169–1211.
11. Andres F. Oberhauser, Carmelu Badilla-Fernandez, Mariano Carrion-Vazquez, and Julio M. Fernandez, *The mechanical hierarchies of fibronectin observed with single-molecule afm*, Journal of Molecular Biology **319** (2002), no. 2, 433 – 447.
12. Dietmar Oelz and Christian Schmeiser, *Derivation of a model for symmetric lamellipodia with instantaneous crosslink turnover*, preprint (2009).
13. ———, *Cell mechanics: from single scale-based models to multiscale modelling*, ch. How do cells move? mathematical modelling of cytoskeleton dynamics and cell migration, Chapman and Hall / CRC Press, to appear, 2009.
14. Dietmar Oelz, Christian Schmeiser, and J. V. Small, *Modelling of the actin-cytoskeleton in symmetric lamellipodial fragments.*, Cell Adhesion and Migration **2** (2008), no. 2, 117–126.
15. B. Rubinstein, K. Jacobson, and A. Mogilner, *Multiscale two-dimensional modeling of a motile simple-shaped cell.*, Multiscale Model. Simul. **3** (2005), no. 2, 413–439.
16. I. Schwaiger, A. Kardinal, M. Schleicher, A.A. Noegel, and M. Rief, *A mechanical unfolding intermediate in an actin-crosslinking protein.*, Nat Struct Mol Biol **11** (2004), no. 21, 81–5.
17. Alexander B. Verkhovsky, Tatyana M. Svitkina, and Gary G. Borisy, *Self-polarization and directional motility of cytoplasm*, Current Biology **9** (1998), no. 1, 11–20.